Environmental Science & Technology

Contaminants in Aquatic and Terrestrial Environments

Dynamics of live oil droplets and natural gas bubbles in deep water

Jonas Gros, J. Samuel Arey, Scott A. Socolofsky, and Anusha L. Dissanayake

Environ. Sci. Technol., **Just Accepted Manuscript** • DOI: 10.1021/acs.est.9b06242 • Publication Date (Web): 28 Aug 2020

Dynamics of live oil droplets and natural gas bubbles in deep water

Authors: Jonas Gros,[a,*] J. Samuel Arey,[b] Scott A. Socolofsky,[c] and Anusha L. Dissanayake[d,1]

[a] GEOMAR Helmholtz Centre for Ocean Research Kiel, RD2/Marine Geosystems, Wischhofstrasse 1-3, D-24148 Kiel, Germany

[b] ExxonMobil Biomedical Sciences Inc., Annandale, NJ 08801, USA

[c] Zachry Department of Civil and Environmental Engineering, Texas A&M University, College Station, TX 77843, USA

[d] RPS Ocean Science, South Kingstown, RI 02879, USA

[1] present address: SINTEF Ocean, Trondheim, Norway

* Corresponding author: jogros@geomar.de. Phone: +49 431 600 2267.

TOC:

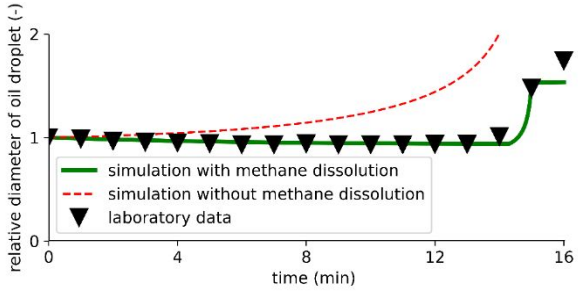

Abstract

Explaining the dynamics of gas-saturated live petroleum in deep water remains a challenge. Recently, Pesch et al. (*Environ. Eng. Sci.* 2018, 35, 289–299) reported laboratory experiments on methane-saturated oil droplets under emulated deep-water conditions, providing an opportunity to elucidate the underlying

dynamical processes. We explain these observations with the Texas A&M Oil spill/Outfall Calculator (TAMOC), which models the pressure-, temperature-, and composition-dependent interactions between: oil-gas phase transfer; aqueous dissolution; and densities and volumes of liquid oil droplets, gas bubbles, and two-phase droplet-bubble pairs. TAMOC reveals that aqueous dissolution removed >95% of the methane from ~3.5-mm live oil droplets within 14.5 min, prior to gas bubble formation, during the experiments of Pesch et al. Additional simulations indicate that aqueous dissolution, fluid density changes, and gas-oil phase transitions (ebullition, condensation) may all contribute to the fates of live oil and gas in deep water, depending on the release conditions. Illustrative model scenarios suggest that 5-mm diameter gas bubbles released at <470 m water depth can transport methane, ethane, and propane to the water surface. Ethane and propane can reach the water surface from much deeper releases of 5-mm diameter live oil droplets, during which ebullition occurs at water depths of <70 m.

Introduction

Petroleum fluids comprised of gaseous and liquid phases may enter deep water through natural seeps,[1–6] small-scale leaks during industry operations,[7] leaking abandoned wells,[8,9] or major accidents such as the *Deepwater Horizon* disaster.[10] During such events, the coupled chemical and physical dynamics of the released gaseous and live liquid petroleum phases largely determine the trajectories and fates of these fluids in the near environment. Whereas the physical behavior of gas bubbles are well-documented,[6,11–20] few direct observations have revealed the chemical and thermodynamic behavior of live liquid petroleum under shallow or deep-water conditions in either the field or the laboratory.[4–6,21–25] Limited field observations have been made on composition, dynamic behavior, ebullition, and oil-to-gas phase transfer,[4–6,25] and laboratory observations have been made on methane-saturated live oil with and

without a pressure drop at the release orifice.[21–24] We define "live" liquid oil as the fluid which occurs as a liquid oil phase at the release depth, and which is comprised of both light and heavy components such that it would occur as two phases, liquid and gas, at water-surface conditions.[26] Live oil contrasts with "dead" liquid oil, which is defined as a fluid sufficiently depleted of light components that it would occur as only a liquid phase at both deep-water and water-surface conditions.

As a consequence of its composition, live liquid oil is potentially susceptible to several thermodynamic and chemical processes in deep water (defined here as >100 m depth) that are distinct from processes expected for dead oil. However, due to the lack of available direct observations, the processes affecting live liquid oil droplets under deep-water conditions have been inferred largely from model predictions. Based on the thermodynamics of petroleum gas-liquid equilibrium under the high-pressure conditions in deep water, C_1–C_5 hydrocarbons may be significantly dissolved in the live liquid oil phase, whereas these compounds would reside primarily in the gas phase at water surface conditions.[25,27–32] Models indicate that several competing processes may subsequently act on these live liquid oil droplets during their ascent through deep water: (1) aqueous dissolution continually transfers C_1–C_5 hydrocarbons (as well as some larger hydrocarbons including BTEX) from ascending droplets into ambient water; (2) the liquid petroleum may become over-saturated with gas due to decreasing ambient pressure, leading to a liquid-to-gas phase transition (ebullition) and partial phase transfer of light components from the petroleum liquid to gas phase; and finally (3) continual changes occur in the densities and volumes of the oil droplets and gas bubbles, which depend on their ongoing changes in pressure, temperature, and compositions.[27,28,33] These coupled processes together also influence the buoyancy, size, and viscosity—and thus vertical rise velocities—of predicted two-phase droplet-bubble pairs,[23,24,28] which are confirmed to exist by observations[5,16,18,23,34–36] (right-most panel of Figure 1b). However, due to the paucity of direct observations in the field or laboratory, the dynamical interplay of these processes for free rising live oil droplets had only been investigated through model simulations[28] until recently.

High-pressure laboratory measurements reported by Pesch et al.[23] provide the first direct, quantitative observations of free rising live oil droplets undergoing the coupled physical and chemical processes that are relevant in deep water. In repeated experiments, these researchers studied an oil droplet that was initially saturated with methane under high pressure conditions and then placed within a counter-current flow channel filled with artificial seawater at high pressure (151 bar). The vertical flow channel kept the droplet in a stationary position while the pressure of the system was decreased at a constant rate. This experimental investigation confirmed that a methane-saturated droplet can evolve gas and thus transition into a two-phase droplet-bubble pair under certain laboratory conditions. In a follow-up study, a similar apparatus has been used by the same team to study conditions with a pressure drop at the release orifice.[24]

In the present study, we show that the published laboratory data[37] of Pesch et al.[23] can be largely explained in terms of phase transition, phase transfer, and mass transfer, which are encoded in the previously validated[11,12,27,28,33,38–40] Texas A&M Oil spill/Outflow Calculator (TAMOC) model.[28,38,41] The present results provide the first validation of the TAMOC model against direct observations of live oil droplets under emulated deep-water conditions, adding new support to key assumptions that were applied in previous simulations of live petroleum fluids released into the deep sea during the *Deepwater Horizon* disaster.[28] Bolstered by this broadened validation, the TAMOC model is then used to explain the physical and chemical controls on the behaviors of C_1–C_3 hydrocarbon compounds in the near-field of the release during *Deepwater Horizon*. Looking ahead, we also explore the conditions that would trigger gas-oil phase transitions in the field, and we evaluate the influence of release depth on these processes.

Methods

Laboratory data of Pesch et al.[23,37] Pesch et al.[23] saturated Louisiana Sweet crude (LSC) oil with pure methane at 151 bar (absolute pressure). A methane-saturated liquid oil droplet of 0.013–0.030 mL was

released into a counter-current flow channel filled with artificial seawater, where it maintained an almost stationary position in a flow of recirculated seawater (Figure 1a). This closed system contained 150 mL of artificial seawater at a constant temperature of 20°C, which had been initially saturated with atmospheric gases at 1 atm (~1 bar) and was absent of methane.[42] Nine independent experiments were conducted using methane-saturated (live) LSC oil, and three experiments were conducted with methane-free (dead) LSC oil. During each of these 12 experiments, the system pressure was steadily decreased until it reached 1 atm, using a constant decompression rate (1, 5, or 10 bar min^{-1}). Overall, four types of experiments (differing in live or dead LSC oil and given decompression rate) were each repeated three times; these triplicates differed only in the initial droplet diameter. The researchers monitored the diameter of the droplet over the course of each experiment (Figure 1b). The duration of each experiment (15, 16, 30, or 150 min) varied depending on the decompression rate.

The Texas A&M Oil spill/Outflow Calculator (TAMOC).[27,28,38] TAMOC is a multiphase buoyant plume modelling suite that simulates the three-dimensional ascent trajectories of live oil droplets, gas bubbles, and two-phase attached droplet-bubble pairs, together with the dynamical changes in their densities, viscosities, and volumes, fully coupled with the processes of gas-oil partitioning, gas-oil phase transitions (ebullition and condensation), and aqueous dissolution kinetics.[27,28,33,43] These processes are parameterized based on pre-existing formulas[12,15,44–61] as previously described[27,28,38] and are explicitly dependent on pressure, temperature, and petroleum composition represented by individual compounds and/or pseudo-components.[27,62] The previously-validated thermodynamic module[27] predicts gas-oil equilibrium partitioning and densities of the gas and liquid oil phases based on the Peng-Robinson equation of state[47,48] with volume translation,[51] a method that is widely accepted by the petroleum industry.[63] The resulting fluid property predictions have been validated for pressures of ≤1,000 bar (corresponding to water depths ≤10,000 m) and temperatures of -2–30°C.[27] TAMOC has been successfully validated for methane bubbles (in the laboratory and field) and for fractionations of C_1–C_{20} compounds

(in the field), based on data encompassing pressure conditions spanning 1 to 151 bar,[11,12,28] as well as for multiphase plume behavior.[38] The key governing equations used in TAMOC for the simulations reported here are described in Supporting Information section S1. The assumptions and boundary conditions for its application to the *Deepwater Horizon* oil spill and to individual live oil droplet and gas bubble simulations are reported in sections S2 and S3.

Application of the TAMOC model to the laboratory conditions of the live oil droplet experiments. The TAMOC code described above was applied to simulate the laboratory experiments by Pesch et al.[23] None of its calibration parameters were modified, and the model setup was appropriately adapted to match the experimental settings (temperature, pressure, salinity, initial droplet diameter, and live-oil composition) and to operate within a fixed volume of seawater. The model simulated the following coupled processes, which were considered relevant during the experiments: the dynamical density, viscosity, and volume changes associated with the live oil droplet or two-phase droplet-bubble pair; gas-oil transition to a two-phase droplet-bubble pair and associated gas-oil partitioning according to the thermodynamic module (described above); and aqueous dissolution kinetics of individual chemical components.[27,28,38,43] These modeled processes are explicitly dependent on pressure, temperature, and petroleum composition.[27,28] A model petroleum composition of 23 chemical components (Table S3 in Gros et al. 2018[62]) was employed to represent LSC oil and methane, based on distillation cut and asphaltene content data available in the ADIOS oil library[64] and various estimation methods.[62,64] The model is predictive and contains no parameters that were tuned using the data reported by Pesch et al.[23]

To initialize the model, the simulated LSC oil was saturated with methane by a gas-oil equilibrium calculation ("flash calculation") at 20°C and 151 bar, which mimicked the laboratory conditions, assuming a gas-to-liquid volume ratio of 1:10 ml ml^{-1} at the flash conditions. This volume ratio ensured that the liquid oil phase was fully saturated with gas at the prescribed conditions. Then, the behavior of this methane-saturated initially-liquid droplet was simulated within a fixed, 150-mL volume of recirculating

seawater subjected to the experimental decompression rate (1, 5, or 10 bar min^{-1}). The kinetics of reversible mass transfers between the petroleum phase(s) and seawater were predicted for water-soluble petroleum components and also for the two major atmospheric gases (N_2 and O_2) initially dissolved in the seawater. The model predicts the evolving composition of seawater, petroleum liquid, and petroleum gas (if present) during the course of the laboratory experiment, including prediction of the formation of a gas phase (if thermodynamically allowed) from the petroleum liquid. In these calculations, the kinetics of mass transfer between petroleum phase(s) and seawater were assumed to follow the rates for "dirty" droplets and bubbles (with suppressed internal circulation) in a quiescent ambient reservoir,[46] consistent with the approximations in our previous simulations of the *Deepwater Horizon* accident.[28] The dirty-interface assumption is consistent with the laboratory observations of Pesch et al.[23] The model further assumes that gas-oil partitioning of the petroleum phases is instantaneous with respect to changing conditions of pressure, temperature, and chemical composition. The assumed instantaneous phase equilibrium within the droplet-bubble pair is supported by field observations of a liquid CO_2 droplet experiencing ebullition and massive phase transfer over 3 m of ascent (12 s) initiated at ~391 m depth,[65,66] where the gas-liquid equilibrium condition corresponded to 397 m depth. In other words, the model assumes that the kinetics of phase transfer between the gas and oil are fast (non-limiting) relative to other processes, whereas the kinetics of mass transfer into water (from either gas or oil) are simulated explicitly (assumed rate-limiting, based on calculations reported in Supporting Information section S4). By assuming gas-oil equilibrium within the droplet-bubble pair, the fugacities are equal in the oil and gas phase. Finally, in the case of oil droplet ebullition, the model assumes that the two ensuing phases (gas and liquid) remain attached together, consistent with the quantitative laboratory observations of Pesch et al.[23] and further supported by qualitative observations at natural seeps.[5,16,18,34–36] As a simplification, the droplet-bubble pair (containing both liquid oil and gas) is assumed to form a sphere, with the two phases joined as two horizontal spherical caps that form the top (gas) or bottom (oil) portions of the sphere.[28] The aggregate

fluid properties of these bi-phasic entities (including interfacial tension with seawater and density) were calculated as reported previously,[28] and are used to calculate derived properties such as rise velocity (Supporting Information section S1).[28]

Results and Discussion

TAMOC simulations explain the observed dynamics of live and dead oil droplets (experiments 1–12). To guide the reader through our interpretation of the Pesch et al.[23] laboratory observations,[37] we first discuss experiments 1–3 in detail. These experiments effectively illuminate the interacting dynamics of several physical and chemical processes affecting live oil droplets, due to an unusually-high decompression rate that takes the system from 151 to 1 bar in just 15 minutes (10 bar min^{-1}). While individual droplets cannot rise at this rate (1.7 m/s), droplets transported in a rising plume above a deep-water blowout may experience these velocities for a short period near the release (section S10).

To represent the averaged conditions of experiments 1–3 of Pesch et al.,[23] the modeled live oil droplet was assigned an initial diameter ($d_{p,0}$) of 3.49 mm. During the initial 13 min of these experiments, the observed live oil droplet diameter shrinks by 5–7%, consistent with the simulated value of 6.0% (Figure 2a), and explained by the model as transfer of 95% of the methane into the water phase by aqueous dissolution (Figure 2c). During this time the system pressure decreases from 151.0 to 21.0 bar (Figure 2b). During the final 3 min of the experiments, the system pressure decreases from 21.0 to 1.0 bar over 2 min and is then held at 1.0 bar for the final 1 min. The observed and simulated droplet diameters both increase significantly (71–98% and 63%, respectively) during these final 3 min, explained by the model as ebullition of methane and other light molecules in the liquid oil to form a gas phase, augmented by gas-volume expansion due to pressure decrease (Figures 2d,e). Overall, the simulated diameter of the live oil droplet

agrees well with the reported observed values over the course of the experiment, exhibiting a root-mean-squared error (RMSE) of 1.3% (Table 1, Figure 2a).

The model reveals that, in experiments 1–3, aqueous dissolution removed 97% of the initially-present methane from the live oil droplet and transferred it into the water within just 16.0 min (Table 1, Figure 2c). This prediction is confirmed by an experimentally-derived estimate of the total depletion of methane (93–96%) from the live oil droplet over the same period, based on a calculation of the methane mass necessary to achieve the reported experimental diameter of the two-phase droplet-bubble pair at the final time point (Table 1). By contrast, if aqueous dissolution of methane is disabled in the simulations, the simulated droplet diameter deviates far above the observed values (Figure 2a), and the RMSE value increases to 104% (Table 1, Figures 2a, S7a).

Validated by the available observations from experiments 1–3, TAMOC simulations provide further insights into the unobserved underlying processes that occurred within the high-pressure vessel. Despite experiencing an extremely rapid decrease in pressure (151.0 to 8.1 bar) during the initial 14.3 min (Figure 2b), the oil droplet did not produce any methane gas: the rapid kinetics of methane dissolution into water prevented the live oil droplet from reaching gas supersaturation and ebullition. In other words, the change in droplet composition brought by aqueous dissolution of methane caused a decrease of the bubble point pressure that outpaced the decrease in system pressure within the experimental vessel (Figures 2b and S13). During this period, the simulated density of the live oil droplet also increased from 752 kg m^{-3} to 840 kg m^{-3} (Figure 2e), due to the loss of 96% of its initial methane content (Figure 2c). After 14.3 min, carrying only 4% of its initial methane, the simulated oil droplet became over-saturated with methane and other dissolved atmospheric gases, due to the 8-fold drop in pressure (8.1 to 1.0 bar, Figure 2b) during the next 0.7 min of the experiment (14.3–15.0 min). This over-saturation produced immediate ebullition followed by equilibrium-controlled transfer of methane (80.1%), N_2 (9.3%), O_2 (4.6%), and other light petroleum compounds (6.1%) from the oil to gas phase (predicted mole percentages reported in the gas at 16 min).

209 This simulated gas bubble contained N_2 and O_2 (in addition to methane) because these atmospheric gases
210 were also present in both the live oil droplet and the seawater.

211 During the final 1.1 min of experiments 1–3, the fast-growing gas phase constituted most of the volume
212 of the two-phase droplet-bubble pair (Figure 2d). According to the model, the rapid expansion of the gas
213 phase during the final 1.7 min (14.3–16.0 min) resulted from two simultaneous effects: the rapid oil-to-
214 gas phase transfer of 70% of the methane remaining in the oil phase to the gas phase (Figure 2c) and a
215 simultaneous 6.7-fold decrease in gas density (Figure 2e), which reached 0.91 kg m^{-3} at 1.0 bar. At 16 min,
216 the simulated volume of gas present relative to the initial droplet volume (2.9) is close to the
217 experimentally-derived values (3.2–5.9) based on data[37] from Pesch et al.[23] (Table 1). The good agreement
218 between simulations and observations during the final 1.7 min validates the model prediction that 96%
219 of the methane in the oil droplet had dissolved into the aqueous phase prior to formation of the methane
220 gas phase. By comparison, neglecting aqueous dissolution leads to model predictions that deviate far from
221 the experimental observation (Table 1, Figures 2 and S7), which confirms the importance of the dissolution
222 process.

223 Finally, ebullition of gas bubbles from the seawater phase was also observed at the very end of experiment
224 2 (right-most panel of Figure 1b). This observation corroborates the TAMOC simulations, which predict
225 supersaturation of aqueously-dissolved gases in the seawater during the final 1.03 min (grey-shaded
226 regions of Figure 2). Apart from this prediction, TAMOC is not designed to explicitly model ebullition from
227 the seawater phase, though it does model the kinetics of mass transfer between seawater and the
228 droplet-bubble pair. Ebullition from the continuous seawater phase is not typically a relevant process in
229 natural environments (discussed further in Supporting Information section S5). However, in experiments
230 1–3, the recruitment of some of these seawater-produced gas bubbles to the live-oil droplet may partly
231 account for the discrepancy between the modeled and observed oil droplet diameter at 16.0 min.

Experiments 1–3 provide an appropriate data set for validating the TAMOC model under laboratory conditions that particularly favor ebullition of gas from live oil. But the rapid decompression rate (10 bar min^{-1}) in these experiments would not normally be encountered by a suspended oil droplet experiencing vertical ascent in deep water due to its buoyancy or by buoyant plume advection. This accelerated decompression rate enhanced the rate and extent of phase transfer from the live oil droplet to gas. In order to emulate the live oil behaviors occurring in deep-water environments, it is more informative to consider experiments 7–9 of Pesch et al.,[23] which employed a decompression rate (1 bar min^{-1}) that more closely resembles realistic field conditions for individual droplets (Figures S10 and S11).

For experiments 4–6 and 7–9, which applied decompression rates of 5 bar min^{-1} and 1 bar min^{-1}, respectively, the modeled live oil droplet diameter agrees reasonably with reported observed values, exhibiting RMSEs of 1.3% and 2.0% (Figures 3a, S8a, and Table 1). TAMOC predicts that >99% of the methane initially present in the liquid oil phase dissolves into the aqueous phase during experiments 4–9 (Figures 3c and S8c), consistent with the empirical estimates (97–99%) deduced from observations (Table 1). For observations near the very end of experiments 4–9 (final 1–10 min, pressures ≤10 bar), the model correctly predicts the formation of a gas phase from the liquid oil but underestimates the observed extent of droplet growth (Figures 3 and S8). Similar to the situation for experiments 1–3 (discussed above), this discrepancy may result from the formation of small gas bubbles throughout the water in the vessel during the final seconds of experiments 4–9 due to gas saturation in the water phase (Figures 3b and S8b), which possibly accelerated the growth of the gas bubble attached to the live oil droplet (Figure 1b, right-most graphic).

Finally, for experiments 10–12 with LSC dead oil (absence of methane), the simulated diameter of the dead oil droplet remains little changed (<0.4% increase) throughout the experiment (Figure S9a). The slight decrease in diameter (3–5%) reported by Pesch et al.[23] remains unexplained (Figure S9a, Table 1).

For all four sets of experimental conditions (experiments 1–12), the TAMOC model successfully explains the reported droplet diameters with RMSE values of ≤2% (Table 1, Figures 2a, 3a, S8a, S9a). TAMOC simulations successfully captured the predominant physical-chemical processes in these experiments, and the model verifies the rapid removal of methane from live oil droplets (experiments 1–9) by aqueous dissolution (Table 1, Figures 2, 3, S7, S8). This conclusion contrasts with that of Pesch et al.,[23,24] who interpreted that aqueous dissolution was a minor process (section S6).

Implications for understanding behaviors of live oil droplets in deep-water conditions. The present study reveals that aqueous dissolution removed 95% of the methane carried by the ~3.5-mm live oil droplets within just 11.5–14.5 min in experiments 1–9 (Figures 2, 3, and S8), prior to onset of ebullition, although these experiments employed conditions that artificially favored ebullition over aqueous dissolution (Supporting Information Section S11). The present study also supports key assumptions of the TAMOC model. Firstly, the ebullition of methane from oil and the subsequent gas-liquid partitioning can both be approximated with thermodynamic equilibria (i.e., the kinetics are fast such that equilibrium can be assumed). This conclusion is based on the observed agreement between the simulated and experimental diameters of the two-phase droplet-bubble pair at the end of experiments 1–3, despite the extreme decompression rate of 10 bar min^{-1}. Secondly, the present work verifies the TAMOC assumption that a two-phase petroleum droplet-bubble pair remains attached after its initial formation. These validations bolster the assumptions that were applied in previous TAMOC simulations of petroleum fluid behaviors for June 8, 2010 in the near-field for the *Deepwater Horizon* disaster site.[28] In the next two sections, we use TAMOC to investigate the behaviors of live oil droplets and gas bubbles under other, more environmentally-realistic conditions.

Role of live oil and gas for the transport of C_1–C_3 compounds during *Deepwater Horizon*. In TAMOC simulations of the situation on June 8, 2010 of the *Deepwater Horizon* disaster, we incorporated a multiphase buoyant plume model of the near-field, such that the predicted total ascent velocities of

simulated droplets and bubbles are determined by their individual slip velocities plus the vertical velocity of the multiphase plume,[67] as described previously.[28] The model set-up and limitations (including the effect of the pressure[24,68] and temperature[27,69] drops and the assumption of initial gas-liquid separation) are discussed in Supporting Information section S2.

Live oil droplet behaviors during *Deepwater Horizon*. During *Deepwater Horizon*, the ascent and aqueous dissolution of C_1–C_3 compounds was predominantly controlled by live oil droplets rather than gas bubbles, according to TAMOC. Assuming a water depth of 1505 m (153 bar and 4.3°C), TAMOC's thermodynamic model predicts that live oil droplets carried 51%, 74%, and 83% of the methane, ethane, and propane that exited the pared Macondo wellhead during the period June 4 – July 15, 2010.[27,28] During their ascent through the deep sea, these liquid oil droplets did not experience significant ebullition, according to TAMOC (Figure 4a). Hence, aqueous dissolution controlled the removal of C_1–C_3 compounds from live oil droplets during June 4 – July 15, and these compounds were consequently chiefly entrapped in the water column based on a simulation for June 8 (Figure 4c).[28] These model predictions (Figure 4c) were validated previously[28] with fractionation indices derived from measurements of C_1–C_3 compounds in the atmosphere[70] and water column[28,69,71] during *Deepwater Horizon*. Subsea dispersant injection (SSDI) at the pared wellhead was applied 94% of the time from June 4 until well shut-in on July 15, 2010,[72] which facilitated the development of small oil droplets (0.1–2.3 mm) near the wellhead according to previously-reported VDROP-J[73] simulations for June 8, 2010,[28] thereby favoring aqueous dissolution. Previously-reported VDROP-J and TAMOC simulations predicted that larger droplets (0.4–7.6 mm) would have formed on June 8, 2010 had SSDI not been applied, leading to 29% of the emitted propane and small amounts of methane and ethane reaching the sea surface.[28] These predictions are consistent with Figure 5 (discussed below), and they illustrate the potential for significant flows of propane to reach the sea surface from a very deep release, depending on the release conditions.

Gas bubble behaviors during *Deepwater Horizon*. All gas bubbles produced immediately above the Macondo wellhead underwent gas-to-liquid transitions (condensation) during their ascent through the deep sea, according to TAMOC (Figure 4b and Supporting Information section S12).[28] These deep-sea bubbles rapidly lost their methane to aqueous dissolution, which caused relative enrichment of ethane and propane and favored condensation of the gas into lightweight liquids, according to simulations. TAMOC predicts that small gas bubbles (<1-mm initial diameter) experienced condensation at heights of <200 m above the release location, whereas gas bubbles having 4-mm initial diameters experienced condensation at heights of 350 m above the release location according to simulations (Figure 4b) for June 8, 2010, during which SSDI was applied. This state change produced liquid droplets that were smaller (Figure 4b) and denser than the originating gas bubbles, resulting in decreased ascent velocities and increased dissolution for each meter of upward travel. The rapid condensation of methane-depleted gas bubbles thus facilitated the ultimate entrapment of C_1–C_3 compounds in the deep sea during this period of the *Deepwater Horizon* disaster (Figure 4c).

Role of live oil and gas for transport of C_1–C_3 compounds during shallow and deep-water releases. To further explore the conditions under which live oil droplets and gas bubbles may transport C_1–C_3 compounds to the sea surface, we conducted additional TAMOC simulations of hypothetical 5-mm diameter oil droplets and gas bubbles that were released at varied water depths ranging from 10 to 1500 m (Supporting Information section S3). A petroleum mixture of fixed composition (23.5% C_1–C_3 and 76.5% LSC oil, by mass) was assumed to equilibrate at each release depth into separate live oil and gas phases, which were simulated as independent live oil droplets and gas bubbles. The assumed separation of oil and gas at release point is partly substantiated by field observation of C_1–C_5 compositions of oil versus gas releases at a natural seep at 3,400 m water depth,[6] though this remains a matter of future research (Supporting Information section S2). As described in section S3, the petroleum mixture was defined by combining a gas containing mole fractions of 83.4% methane, 9.9% ethane and 6.7% propane with LSC oil

such that the simulated in-situ gas-to-oil volume ratio was 0.4 at 1500 m water depth (153 bar and 4.3°C). This petroleum fluid composition represents a typical light sweet live crude oil, in which the distribution of C_1–C_3 compounds represents a typical wet natural gas.[74] To provide a screening-level assessment with simplified hydrodynamics, the buoyant plume dynamics created by entrained water were not included in the model. Hence these simulations approximate small quiescent releases like most natural seeps and some types of small leaks from operation infrastructure, which usually generate weak bubble plumes[75] leading to limited vertical acceleration of bubbles and droplets.

First, we simulated 5 mm-diameter droplets of live LSC oil (containing 0.8–49.5% methane, 0.6–8.8% ethane and 1.3–8.8% propane, by mole) that were released at water depths ranging from 10 to 1500 m (Figures 5a–c, SI section S3). For these cases, TAMOC predicts that live oil droplets would transport 6–56% of the total released propane to the sea surface, depending on the release depth (10–1500 m), whereas 1–12% of the total released ethane would be transported to the sea surface by 5-mm droplets released from depths of 10–1260 m (Figure 5f). By comparison, live oil droplets do not transport a meaningful fraction of the total released methane to the water surface, regardless of the release depth. TAMOC predicts that these large live oil droplets experience ebullition upon reaching depths of <70 m (Figure 5a), driven by ethane and propane. For example, after release from 500 m water depth, a live oil droplet is predicted to undergo ebullition at 19 m depth (Figure 5a), while still carrying 56% of the total released propane and 10% of the total released ethane (Figure 5c). After ebullition, the predicted gas volume reaches up to 5.3× the initial droplet volume (Figure 5b), which accelerates the ascent of the droplet-bubble pair to the water surface. These predictions depend on the simulated initial droplet size, initial fluid composition, and other conditions at the release site. However, they reveal that live oil droplets can effectively transport ethane and propane to the sea surface from a wide range of release depths (Figure 5f), subject to the interacting processes of aqueous dissolution, ebullition, and changing fluid densities and compositions.

Second, we conducted TAMOC simulations of hypothetical 5 mm-diameter gas bubbles containing C_1–C_3, (mole fractions of 81.3–91.8% methane, 5.8–9.6% ethane and 2.0–6.1% propane) at release depths ranging from 10 to 1500 m (Figures 5d–e, SI section S3). TAMOC predicts that gas bubble releases from >470 m water depth would condense into lightweight liquids (510–640 kg m^{-3}) at heights of 210–410 m above the release point, which correspond to water depths of 1290 to 60 m (Figure 5d). By the time these gas bubbles underwent condensation (defined here as becoming >1% liquid by volume, or >2.9–46% liquid by mass), they had lost 45–99.6% of their initial C_1–C_3 mass to aqueous dissolution. These newly formed liquid droplets were smaller and denser. Bubbles released at shallower water depths bring increasing fractions of the total released C_1–C_3 to the sea surface with decreasing release depth: up to 89–92% for a release at 10-m water depth (Figure 5f). These results depend on the initial petroleum fluid composition, release depths, and initial bubble size (assumed here: 5 mm). However, overall, gas bubble condensation slows the upward ascent of C_1–C_3 compounds and thereby increases their entrapment by aqueous dissolution in deep water, which can decrease or prevent the arrival of these compounds at the water surface.

We conclude that live oil droplets and gas bubbles in deep water can undergo aqueous dissolution of C_1–C_3 compounds, fluid density changes, phase transitions (ebullition, condensation), and gas-oil phase transfer (repartitioning). These processes depend on the water depth of the release, initial size distributions of released droplets and bubbles, and released fluid composition. Releases with high flow rates (such as well blowouts) usually produce an initial multiphase momentum- and buoyancy-driven plume of oil, gas, and entrained seawater (simulated for Figure 4 but not for Figure 5), which may further influence the transport of petroleum fluids in the water column. Results of the present work demonstrate that these processes should be included in scenario models that are used to support risk assessment and emergency response for underwater releases of live oil and gas.

373

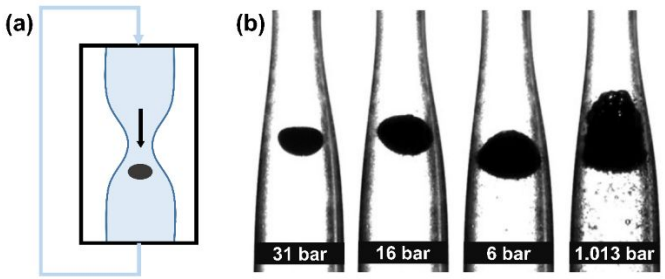

374

375 *Figure 1. (a) Schematic depiction of the experimental device used by Pesch et al.:[23] an oil droplet is maintained stationary within*
376 *a counter-current flow channel containing recirculated seawater under high pressure. A detailed description of the experimental*
377 *set-up is provided in the original publication.[23] (b) Photo taken during the last three minutes of laboratory experiment 2 of Pesch*
378 *et al.[23] before reaching atmospheric pressure (1.013 bar), for a droplet exposed to a decompression rate of 10 bar min^{-1} (absolute*
379 *pressures are indicated). Panel (b) is reproduced from Pesch et al.[23] with permission.*

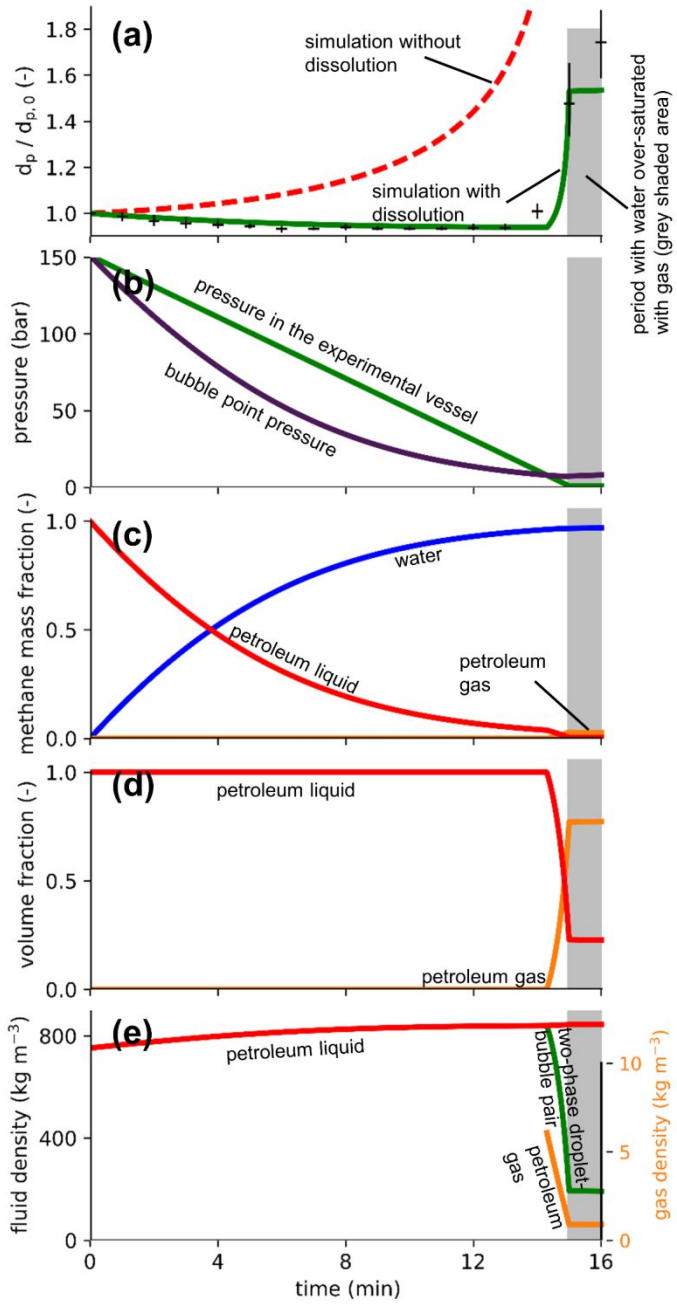

Figure 2. Simulated and experimental results for methane-saturated LSC oil droplets in experiments 1–3 of Pesch et al.[23,37] (a) Relative diameter of oil droplets in experiments 1–3: TAMOC simulations (solid green line) are compared to laboratory observations of Pesch et al.[23,37] (black crosses: the horizontal line displays the arithmetic average; the vertical line indicates the measured range spanned by 3 experiments). Also shown are results of TAMOC simulations with aqueous dissolution suppressed (red dashed line). (b) Absolute pressure within the experimental vessel (green line, decompression rate of 10 bar min^{-1}) and simulated bubble point pressure at the experimental temperature of 20°C (purple line). Also see Fig. S13. (c) Modeled mass fractions of total methane in the experimental vessel: dissolved in seawater (blue line), dissolved in oil liquid (red line), and gaseous (orange line). (d) Modeled fractions of total volume of the droplet-bubble pair represented by oil liquid (red line) and gas (orange line). (e) Modeled oil density (red line, left axis), aggregate density of the bi-phasic droplet-bubble pair (green line, left axis), and gas-phase density (orange line, right axis). All panels: the grey-shaded areas indicate the period during which the vessel water was predicted by TAMOC to be over-saturated with gases, which would explain the spontaneous formation of a gas phase that is observed in the vessel water during the final minutes of the experiment (this phase transition was not simulated).

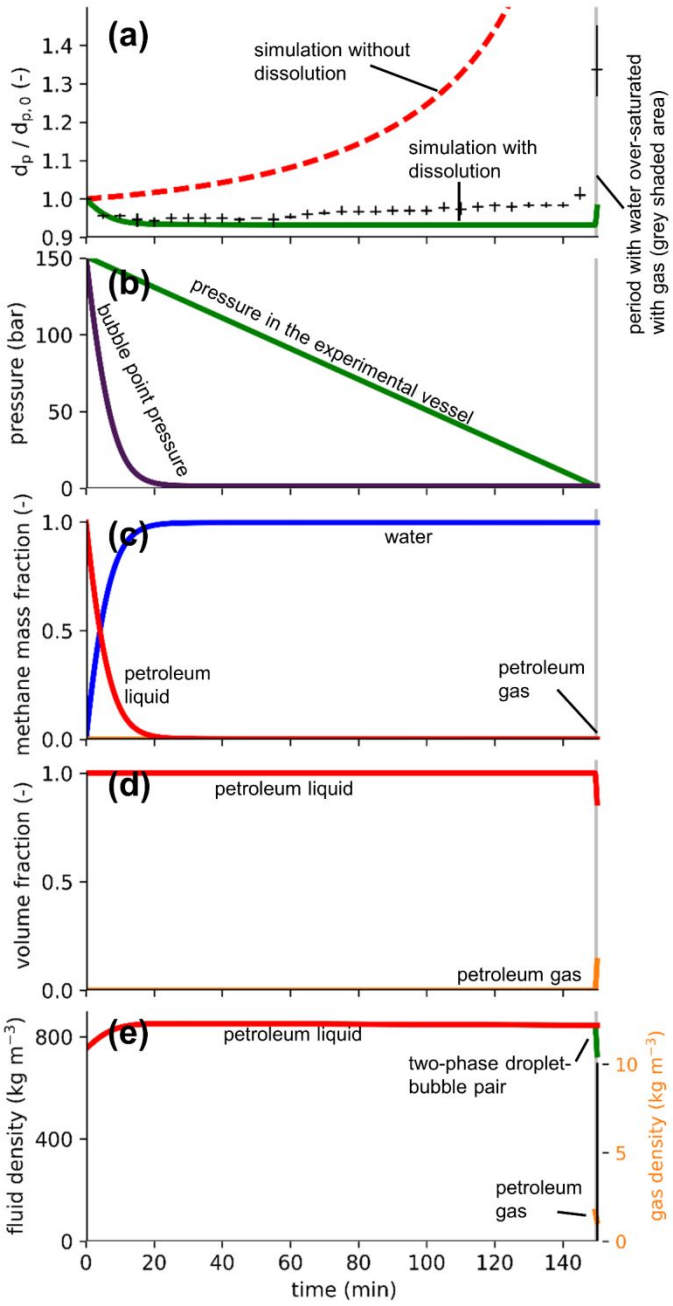

393

394 *Figure 3. Simulated and experimental results for methane-saturated LSC oil droplets in experiments 7–9 of Pesch et al.[23,37] (a)*
395 *Relative diameter oil droplets in experiments 7–9: TAMOC simulations (solid green line) are compared to laboratory observations*
396 *of Pesch et al.[23,37] (black crosses: the horizontal line displays the arithmetic average; the vertical line indicates the measured range*
397 *spanned by 3 experiments). Also shown are results of TAMOC simulations with aqueous dissolution suppressed (red dashed line).*
398 *(b) Absolute pressure within the experimental vessel (green line, decompression rate of 1 bar min^{-1}) and simulated bubble point*
399 *pressure at the experimental temperature of 20°C (purple line). Also see section S12. (c) Modeled mass fractions of total methane*
400 *in the experimental vessel: dissolved in seawater (blue line), dissolved in oil liquid (red line), and gaseous (orange line). (d) Modeled*
401 *fraction of total volume of the droplet-bubble pair represented by oil liquid (red line) and gas (orange line). (e) Modeled oil density*
402 *(red line, left axis), aggregate density of the bi-phasic droplet-bubble pair (green line, left axis), and gas-phase density (orange*
403 *line, right axis). All panels: the grey-shaded areas indicate the period during which the vessel water was predicted by TAMOC to*
404 *be over-saturated with gases (final 28 s of the experiment), which may have led to the spontaneous formation of a gas phase*
405 *during the final seconds of the experiment (this phase transition was not simulated).*

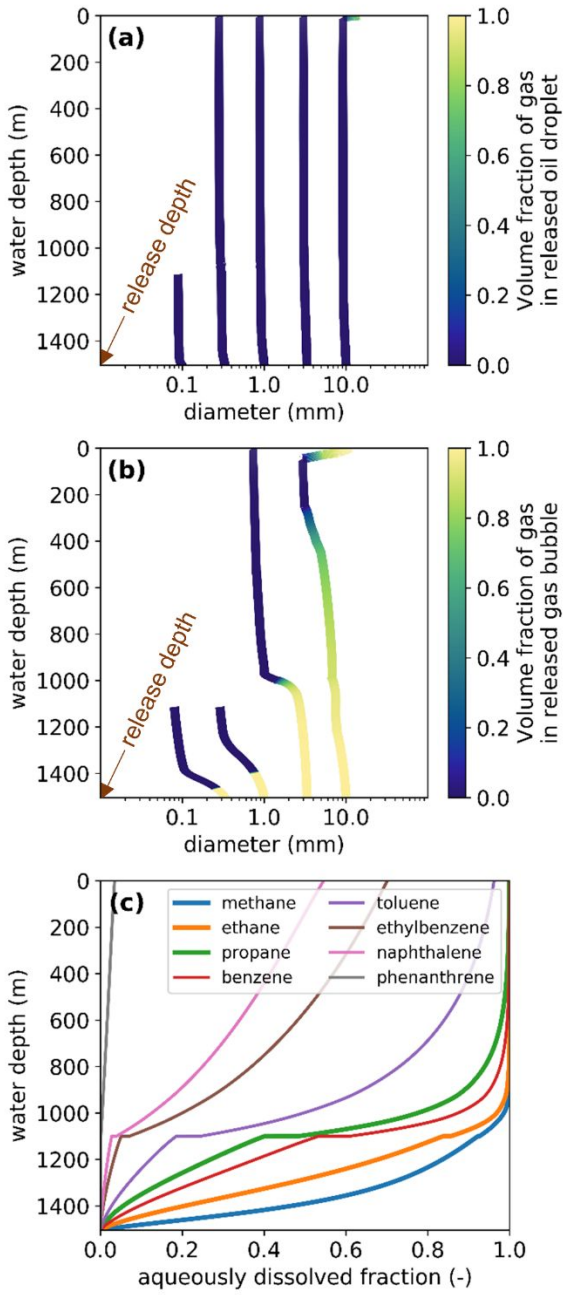

406

407 *Figure 4. TAMOC model predictions of oil droplets and gas bubbles released from the pared Macondo wellhead at 1505 m depth*
408 *on June 8, 2010, of the Deepwater Horizon disaster. (a) Volume fraction of gas in initially-liquid live oil droplets during their ascent*
409 *through the water column. Trajectories are shown for oil droplets having initial diameters ranging from 100 µm to 10 mm. (b)*
410 *Volume fraction of gas in initially-gaseous bubbles during their upward trajectories through the water column, showing results*
411 *for bubbles having initial diameters ranging from 333 µm to 10 mm. These simulations were conducted assuming non-circulating*
412 *interfaces ("dirty"), consistent with the laboratory observations of Pesch et al.[23] The trajectories of droplets and bubbles were*
413 *modeled until they reached the sea surface; for cases in which the droplets/bubbles exhibited insufficient ascent velocities to*
414 *escape the deep-water intrusion (900–1,300 m depth) within 10 h from their release, trajectories were simulated only until the*
415 *deep-water intrusion depth. (c) Total extent of dissolution into the ambient water column, with respect to depth, for methane,*
416 *ethane, propane, and a selection of larger aromatic hydrocarbons on June 8, 2010 (with SSDI), according to TAMOC (84% of the*
417 *mass of Macondo dead oil was constituted of compounds having an aqueous solubility lower or equal to that of phenanthrene).*
418 *All the aqueous dissolution happening within 1,500–900 m depth was channeled to the deep-water hydrocarbon-rich intrusion.*

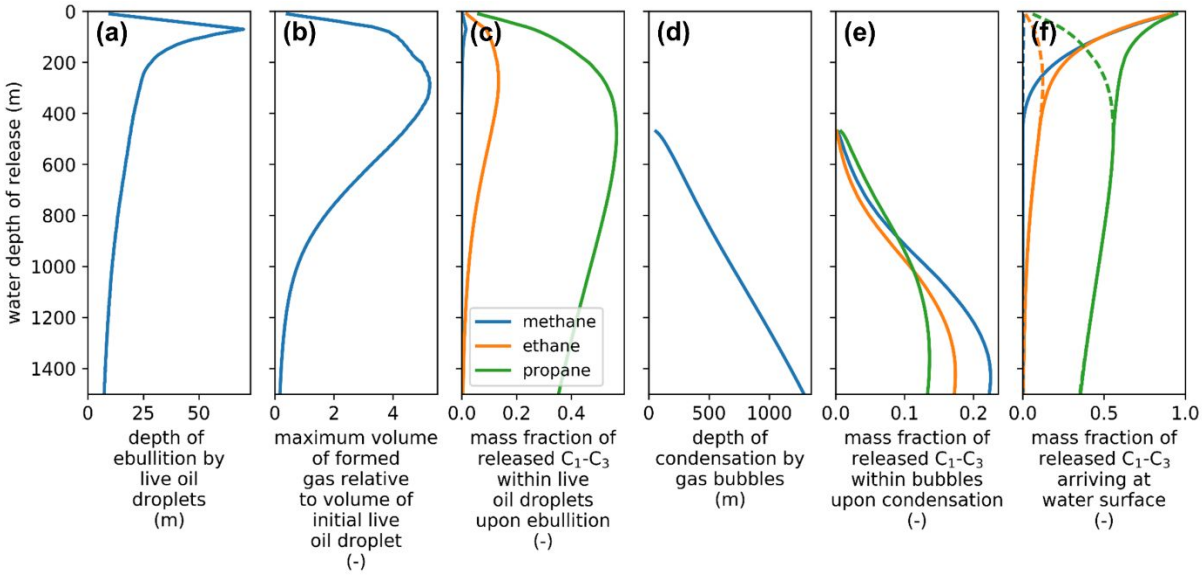

Figure 5. Behaviors of simulated LSC live oil droplets (panels a–c) and gas bubbles (panels d–e), for releases at varying water depths ranging from 10 to 1500 m in the Gulf of Mexico, assuming a release of a LSC reservoir fluid containing 16.3% methane, 3.64% ethane, and 3.58% propane by mass. The initial diameters of both the simulated droplets and bubbles were 5 mm. Their initial compositions were determined by a gas-oil equilibrium calculation at the temperature and pressure conditions prevailing at release depth (SI section S3). For gas bubbles, condensation is defined as the presence of >1% liquid by volume, i.e. 2.9–46% liquid by mass). The depicted mass fractions of the total released C_1–C_3 compounds within (c) droplets upon ebullition and (e) bubbles upon condensation are determined as: C_x mass in the droplet (or bubble) relative to C_x mass in the whole reservoir fluid. (f) The predicted total mass fractions of methane, ethane, and propane that arrive at the sea surface (i.e., the mass fraction not removed from oil droplets and gas bubbles by aqueous dissolution) for releases at varying water depths. On panel f, the dashed line represent the contribution of live oil droplets, whereas the solid lines represent the overall contribution of both droplets and bubbles.

Table 1. Comparison of TAMOC predictions with laboratory observations reported by Pesch et al.[23,37] for live and dead oil droplets (Experiments 1–12). Also shown are model values when assuming suppressed aqueous dissolution of methane.

Experiment no.	1–3	4–6	7–9	10–12
Decompression rate, bar min^{-1}	10	5	1	10
Average initial diameter $d_{P,0}$ and range of values for the three replicate experiments (in parenthesis), mm	3.49 (3.22–3.79)	3.08 (2.95–3.32)	3.71 (3.47–3.86)	4.41 (4.38–4.45)
RMSE[a] of TAMOC-simulated d_p values versus laboratory observations of Pesch et al.[23]	1.3%	1.3%	2.0%	1.8%
RMSE[a,b] of TAMOC-simulated d_p values with suppressed aqueous dissolution versus laboratory observations of Pesch et al.[23]	104%	73%	70%	–[h]
Relative volume[c] of final gas – Experimental value[d]	3.2–5.9	0.7–1.3	1.3–2.3	–[h]
Relative volume[c] of final gas – Simulated value (TAMOC)[e]	2.9	0.08	0.16	–[h]
Relative volume[c] of final gas – Value with suppressed aqueous dissolution of methane (TAMOC)[f]	89	89	89	–[h]
Fraction of methane that became aqueously dissolved during the experiment – Estimated from laboratory data[g]	93–96%	98–99%	97–98%	–[h]
Fraction of methane that became aqueously dissolved during the experiment – Simulated (TAMOC)[e]	97%	99.8%	99.7%	–[h]

[a] Root-mean-squared error (RMSE) values were calculated for all available observation data taken during the periods when vessel water was predicted by TAMOC to be under-saturated with dissolved gases (i.e., excluding gray-shaded areas on Figures 2a, 3a, and S8a). RMSE values are expressed as a percentage of the initial droplet diameter.

[b] The vessel water never becomes over-saturated with gases during the TAMOC simulation with suppressed aqueous dissolution of methane.

[c] Relative volume of final gas = gas volume at the end of the experiment divided by the initial live oil droplet volume at the start of the experiment.

[d] For the experimentally-derived estimate, we assumed that the relative volume of final gas (V_{gas}) could be determined from the observed relative final volume of the bi-phasic droplet-bubble pair ($V_{end,tot}$) and the relative final volume of liquid dead oil ($V_{dead\ oil}$, deduced from observations) according to: $V_{gas} = V_{end,tot} - V_{dead\ oil}$, where $V_{end\ tot}$ was determined by the relative diameter (ratio of measured diameter to the initial droplet diameter) of the droplet-bubble pair reported by Pesch et al.[23,37] at the last measurement they performed. Values of $V_{dead\ oil}$ are smaller than the initial droplet volume at the start of the experiment due to methane aqueous dissolution; $V_{dead\ oil}$ was determined from the smallest relative diameter observed at any time point in the experiment by Pesch et al.,[23,37] assuming that any subsequent diameter increase was caused by ebullition. The smallest relative diameter reported was 0.92±0.01, leading to $V_{dead\ oil}$ = 0.779±0.025; this value is consistent with TAMOC predictions for experiments 1–9 (0.80–0.82).

[e] Simulated value at the end of the experiment of Pesch et al.[23]

[f] This result is based on two Peng-Robinson Equation-of-State (PR EOS) calculations of methane-saturated live oil at 20°C and 151 and 1.01325 bar, respectively. Based on the first of these calculations, the initial methane content in the live oil at the beginning of the experiment of Pesch et al.[23] was estimated to be 56.9 kg m^{-3}, which is reasonably close to the 42.3 kg m^{-3} assumed by Pesch et al.[23] based on laboratory data by Jaggi et al.[76] for a similar light oil (methane-saturated Macondo dead oil). The second PR EOS calculation provided the gas and oil volumes after the mixture was brought to 1.01325 bar.

[g] This value was estimated as the calculated quantity of methane needed to reach the observed $d_P/d_{P,0}$ value at the last measurement in the experiment, based on a TAMOC gas-oil equilibrium calculation at 1.0 bar and 20°C. This calculation neglected the small amount of nitrogen and oxygen present in the gas and oil.

[h] Dead oil simulation, assuming absence of methane.

Supporting Information

Extended description of the TAMOC model; assumptions for the simulations of the *Deepwater Horizon* nearfield on June 8, 2010; assumptions for the simulation of live oil droplets and gas bubbles in the sea; quantitative evaluation of the phases driving mass transfer limitation; discussion of gas supersaturation in the vessel water of the experimental device of Pesch et al.;[23] graphics of TAMOC simulation of experiments 1–3 of Pesch et al.[23] with suppressed aqueous dissolution of methane; graphics of TAMOC simulation of experiments 4–6 and 10–12 of Pesch et al.;[23] live and dead oil droplet ascent velocities; predicted vertical velocity of the plume during *Deepwater Horizon*; discussion of why the conditions selected for the experiments of Pesch et al.[23] favored ebullition of the live oil droplets; comparison of phase behaviors for single-component versus multi-component fluids and simulated phase envelopes.

Acknowledgements

We gratefully acknowledge Simeon Pesch (TUHH) for clarification about his experimental setup, Deborah French-McCay (RPS ASA) for discussion of conditions during *Deepwater Horizon*, and Peter Walz, Peter Brewer, and Edward Pelzer (MBARI) for sharing information about their field experiments.[25,65] The comments of the two anonymous reviewers helped improve the manuscript. This project was made possible in part by a grant from The Gulf of Mexico Research Initiative to the Center for Integrated Modeling and Analysis of the Gulf Ecosystem (C-IMAGE) Consortium. Data are publicly available through the Gulf of Mexico Research Initiative Information & Data Cooperative (GRIIDC) (at https://data.gulfresearchinitiative.org, https://doi.org/10.7266/PSTFE3GN for the simulations of the Pesch et al.[23] laboratory experiments, https://doi.org/10.7266/N79885GB[37] for the laboratory data of

Pesch et al.,[23] and https://doi.org/10.7266/N7DF6P8R for the simulations of June 8, 2010 of the *Deepwater Horizon*.[28,43] The latest version of the TAMOC model source code is publicly available at: https://github.com/socolofs/tamoc.

References

(1) Körber, J.-H.; Sahling, H.; Pape, T.; dos Santos Ferreira, C.; MacDonald, I.; Bohrmann, G. Natural Oil Seepage at Kobuleti Ridge, Eastern Black Sea. *Marine and Petroleum Geology* **2014**, *50*, 68–82. https://doi.org/10.1016/j.marpetgeo.2013.11.007.

(2) Jiang, K.; Zhang, J.; Sakatoku, A.; Kambayashi, S.; Yamanaka, T.; Kanehara, T.; Fujikura, K.; Pellizari, V. H. Discovery and Biogeochemistry of Asphalt Seeps in the North São Paulo Plateau, Brazilian Margin. *Scientific Reports* **2018**, *8* (1), 12619. https://doi.org/10.1038/s41598-018-30928-2.

(3) MacDonald, I. R.; Garcia-Pineda, O.; Beet, A.; Asl, S. D.; Feng, L.; Graettinger, G.; French-McCay, D.; Holmes, J.; Hu, C.; Huffer, F.; Leifer, I.; Muller-Karger, F.; Solow, A.; Silva, M.; Swayze, G. Natural and Unnatural Oil Slicks in the Gulf of Mexico. *Journal of Geophysical Research: Oceans* **2015**, *120* (12), 8364–8380. https://doi.org/10.1002/2015JC011062.

(4) Leifer, I.; Wilson, K.; Tarpley, J.; Lewis, R.; Imai, R.; Sowby, M.; Mayer, K.; Moore, C. Factors Affecting Marine Hydrocarbon Emissions in an Area of Natural Seeps and Abandoned Oil Wells - Summerland, California. *International Oil Spill Conference Proceedings* **2005**, *2005* (1), 849–853. https://doi.org/10.7901/2169-3358-2005-1-849.

(5) Leifer, I. A Synthesis Review of Emissions and Fates for the Coal Oil Point Marine Hydrocarbon Seep Field and California Marine Seepage. *Geofluids* **2019**, 48. https://doi.org/10.1155/2019/4724587.

(6) Römer, M.; Hsu, C.-W.; Loher, M.; MacDonald, I. R.; dos Santos Ferreira, C.; Pape, T.; Mau, S.; Bohrmann, G.; Sahling, H. Amount and Fate of Gas and Oil Discharged at 3400 m Water Depth From a Natural Seep Site in the Southern Gulf of Mexico. *Front. Mar. Sci.* **2019**, *6*. https://doi.org/10.3389/fmars.2019.00700.

(7) Vinnem, J. E.; Hestad, J. A.; Kvaløy, J. T.; Skogdalen, J. E. Analysis of Root Causes of Major Hazard Precursors (Hydrocarbon Leaks) in the Norwegian Offshore Petroleum Industry. *Reliability Engineering & System Safety* **2010**, *95* (11), 1142–1153. https://doi.org/10.1016/j.ress.2010.06.020.

(8) Vielstädte, L.; Karstens, J.; Haeckel, M.; Schmidt, M.; Linke, P.; Reimann, S.; Liebetrau, V.; McGinnis, D. F.; Wallmann, K. Quantification of Methane Emissions at Abandoned Gas Wells in the Central North Sea. *Mar. Petrol. Geol.* **2015**, *68*, 848–860. https://doi.org/10.1016/j.marpetgeo.2015.07.030.

(9) Vielstädte, L.; Haeckel, M.; Karstens, J.; Linke, P.; Schmidt, M.; Steinle, L.; Wallmann, K. Shallow Gas Migration along Hydrocarbon Wells–An Unconsidered, Anthropogenic Source of Biogenic Methane in the North Sea. *Environ. Sci. Technol.* **2017**, *51* (17), 10262–10268. https://doi.org/10.1021/acs.est.7b02732.

(10) McNutt, M. K.; Camilli, R.; Crone, T. J.; Guthrie, G. D.; Hsieh, P. A.; Ryerson, T. B.; Savas, O.; Shaffer, F. Review of Flow Rate Estimates of the *Deepwater Horizon* Oil Spill. *PNAS* **2012**, *109* (50), 20260–20267. https://doi.org/10.1073/pnas.1112139108.

(11) Leonte, M.; Wang, B.; Socolofsky, S. A.; Mau, S.; Breier, J. A.; Kessler, J. D. Using Carbon Isotope Fractionation to Constrain the Extent of Methane Dissolution into the Water Column Surrounding a Natural Hydrocarbon Gas Seep in the Northern Gulf of Mexico. *Geochem. Geophy. Geosy.* **2018**, *19* (11), 4459–4475. https://doi.org/10.1029/2018GC007705.

(12) Jun, I. A Numerical Model for Hydrocarbon Bubbles from Natural Seeps within Hydrate Stability Zone. Ph.D. Dissertation, Texas A&M University, College Station, Texas, 2018.

(13) Römer, M.; Sahling, H.; Pape, T.; Bohrmann, G.; Spieß, V. Quantification of Gas Bubble Emissions from Submarine Hydrocarbon Seeps at the Makran Continental Margin (Offshore Pakistan). *Journal of Geophysical Research: Oceans* **2012**, *117* (C10). https://doi.org/10.1029/2011JC007424.

(14) Rehder, G.; Leifer, I.; Brewer, P. G.; Friederich, G.; Peltzer, E. T. Controls on Methane Bubble Dissolution inside and Outside the Hydrate Stability Field from Open Ocean Field Experiments and Numerical Modeling. *Marine Chemistry* **2009**, *114* (1–2), 19–30. https://doi.org/10.1016/j.marchem.2009.03.004.

(15) McGinnis, D. F.; Greinert, J.; Artemov, Y.; Beaubien, S. E.; Wüest, A. Fate of Rising Methane Bubbles in Stratified Waters: How Much Methane Reaches the Atmosphere? *J. Geophys. Res.* **2006**, *111* (C9), C09007. https://doi.org/10.1029/2005JC003183.

(16) Johansen, C.; Todd, A. C.; MacDonald, I. R. Time Series Video Analysis of Bubble Release Processes at Natural Hydrocarbon Seeps in the Northern Gulf of Mexico. *Marine and Petroleum Geology* **2017**, *82*, 21–34. https://doi.org/10.1016/j.marpetgeo.2017.01.014.

(17) Wang, B.; Socolofsky, S. A.; Breier, J. A.; Seewald, J. S. Observations of Bubbles in Natural Seep Flares at MC 118 and GC 600 Using in Situ Quantitative Imaging. *Journal of Geophysical Research: Oceans* **2016**, *121* (4), 2203–2230. https://doi.org/10.1002/2015JC011452.

(18) De Beukelaer, S. M.; MacDonald, I. R.; Guinnasso, N. L.; Murray, J. A. Distinct Side-Scan Sonar, RADARSAT SAR, and Acoustic Profiler Signatures of Gas and Oil Seeps on the Gulf of Mexico Slope. *Geo-Mar Lett* **2003**, *23* (3), 177–186. https://doi.org/10.1007/s00367-003-0139-9.

(19) Riedel, M.; Scherwath, M.; Römer, M.; Veloso, M.; Heesemann, M.; Spence, G. D. Distributed Natural Gas Venting Offshore along the Cascadia Margin. *Nature Communications* **2018**, *9* (1), 3264. https://doi.org/10.1038/s41467-018-05736-x.

(20) Clarke, R. H.; Cleverly, R. W. Petroleum Seepage and Post-Accumulation Migration. *Geological Society, London, Special Publications* **1991**, *59* (1), 265–271. https://doi.org/10.1144/GSL.SP.1991.059.01.17.

(21) Brandvik, P. J.; Storey, C.; Davies, E. J.; Johansen, Ø. Combined Releases of Oil and Gas under Pressure; the Influence of Live Oil and Natural Gas on Initial Oil Droplet Formation. *Marine Pollution Bulletin* **2019**, *140*, 485–492. https://doi.org/10.1016/j.marpolbul.2019.01.036.

(22) Malone, K.; Pesch, S.; Schlüter, M.; Krause, D. Oil Droplet Size Distributions in Deep-Sea Blowouts: Influence of Pressure and Dissolved Gases. *Environ. Sci. Technol.* **2018**, *52* (11), 6326–6333. https://doi.org/10.1021/acs.est.8b00587.

(23) Pesch, S.; Jaeger, P.; Jaggi, A.; Malone, K.; Hoffmann, M.; Krause, D.; Oldenburg, T. B. P.; Schlüter, M. Rise Velocity of Live-Oil Droplets in Deep-Sea Oil Spills. *Environ. Eng. Sci.* **2018**, *35* (4), 289–299. https://doi.org/10.1089/ees.2017.0319.

(24) Pesch, S.; Schlüter, M.; Aman, Z. M.; Malone, K.; Krause, D.; Paris, C. B. Behavior of Rising Droplets and Bubbles: Impact on the Physics of Deep-Sea Blowouts and Oil Fate. In *Deep Oil Spills: Facts, Fate, and Effects*; Murawski, S. A., Ainsworth, C. H., Gilbert, S., Hollander, D. J., Paris, C. B., Schlüter, M., Wetzel, D. L., Eds.; Springer International Publishing: Cham, 2020; pp 65–82. https://doi.org/10.1007/978-3-030-11605-7_5.

(25) Peltzer, E. T.; Sauthoff, W.; Walz, P. M.; Brewer, P. G. Deep-Sea Observations of a Rising Methane Saturated Decane Plume within the Hydrate Phase Space. In *Proceedings of the 8th International Conference on Gas Hydrates (ICGH8-2014)*; Beijing, China, 2014.

(26) Ahmed, T. *Reservoir Engineering Handbook*, 4th ed.; Elsevier: Burlington, 2010.

(27) Gros, J.; Reddy, C. M.; Nelson, R. K.; Socolofsky, S. A.; Arey, J. S. Simulating Gas–Liquid–Water Partitioning and Fluid Properties of Petroleum under Pressure: Implications for Deep-Sea Blowouts.

Environmental Science & Technology **2016**, *50* (14), 7397–7408. https://doi.org/10.1021/acs.est.5b04617.

(28) Gros, J.; Socolofsky, S. A.; Dissanayake, A. L.; Jun, I.; Zhao, L.; Boufadel, M. C.; Reddy, C. M.; Arey, J. S. Petroleum Dynamics in the Sea and Influence of Subsea Dispersant Injection during *Deepwater Horizon*. *PNAS* **2017**, 201612518. https://doi.org/10.1073/pnas.1612518114.

(29) Zick, A. A. *Equation-of-State Fluid Characterization and Analysis of the Macondo Reservoir Fluids*; Expert report prepared on behalf of the United States TREX-011490R; 2013.

(30) Zick, A. A. *Expert Rebuttal Report*; prepared on behalf of the United States TREX-011491R; 2013.

(31) Fingas, M. Chapter 15. Deepwater Horizon Well Blowout Mass Balance. In *Oil Spill Science and Technology*; Gulf Professional Publishing (Elsevier): Cambridge (USA) and Oxford (UK), 2017; p 1078.

(32) Camilli, R.; Iorio, D. D.; Bowen, A.; Reddy, C. M.; Techet, A. H.; Yoerger, D. R.; Whitcomb, L. L.; Seewald, J. S.; Sylva, S. P.; Fenwick, J. Acoustic Measurement of the *Deepwater Horizon* Macondo Well Flow Rate. *PNAS* **2012**, *109* (50), 20235–20239. https://doi.org/10.1073/pnas.1100385108.

(33) Socolofsky, S. A.; Dissanayake, A. L.; Jun, I.; Gros, J.; Arey, J. S.; Reddy, C. M. Texas A&M Oilspill Calculator (TAMOC) Modeling Suite for Subsea Spills. In *Proceedings of the Thirty-Eighth AMOP Technical Seminar*; Environment Canada: Ottawa, 2015; pp 153–168.

(34) Padilla, A. M.; Loranger, S.; Kinnaman, F. S.; Valentine, D. L.; Weber, T. C. Modern Assessment of Natural Hydrocarbon Gas Flux at the Coal Oil Point Seep Field, Santa Barbara, California. *Journal of Geophysical Research: Oceans* **2019**, *124* (4), 2472–2484. https://doi.org/10.1029/2018JC014573.

(35) Leifer, I.; MacDonald, I. Dynamics of the Gas Flux from Shallow Gas Hydrate Deposits: Interaction between Oily Hydrate Bubbles and the Oceanic Environment. *Earth and Planetary Science Letters* **2003**, *210* (3), 411–424. https://doi.org/10.1016/S0012-821X(03)00173-0.

(36) MacDonald, I. R.; Leifer, I.; Sassen, R.; Stine, P.; Mitchell, R.; Guinasso, N. Transfer of Hydrocarbons from Natural Seeps to the Water Column and Atmosphere. *Geofluids* **2002**, *2* (2), 95–107. https://doi.org/10.1046/j.1468-8123.2002.00023.x.

(37) Schlüter, M.; Pesch, S. Expansion of Gas-Saturated Crude Oil Droplets, 2017. https://doi.org/10.7266/N79885GB.

(38) Dissanayake, A. L.; Gros, J.; Socolofsky, S. A. Integral Models for Bubble, Droplet, and Multiphase Plume Dynamics in Stratification and Crossflow. *Environ. Fluid Mech.* **2018**, 1–36. https://doi.org/10.1007/s10652-018-9591-y.

(39) Dissanayake, A. L.; Jun, I.; Socolofsky, S. A. Numerical Models to Simulate Oil and Gas Blowout Plumes and Associated Chemical and Physical Processes of Hydrocarbons. In *E-Proceedings of the 36th IAHR World Congress*; The Hague, 2015.

(40) Gros, J.; Schmidt, M.; Dale, A. W.; Linke, P.; Vielstädte, L.; Bigalke, N.; Haeckel, M.; Wallmann, K.; Sommer, S. Simulating and Quantifying Multiple Natural Subsea CO_2 Seeps at Panarea Island (Aeolian Islands, Italy) as a Proxy for Potential Leakage from Subseabed Carbon Storage Sites. *Environ. Sci. Technol.* **2019**, *53* (17), 10258–10268. https://doi.org/10.1021/acs.est.9b02131.

(41) Socolofsky, S. A. *TAMOC*; College Station, 2017.

(42) Pesch, S. Hamburg University of Technology, Hamburg, Germany. Personal Communication, 2018.

(43) Socolofsky, S. A.; Gros, J.; Zhao, L.; Boufadel, M. C. Research Version of the Texas A&M Oil Spill (Outfall) Calculator (TAMOC) and Input Files, 2016. https://doi.org/10.7266/n7df6p8r.

(44) Kumar, A.; Hartland, S. Correlations for Prediction of Mass Transfer Coefficients in Single Drop Systems and Liquid–Liquid Extraction Columns. *Chem. Eng. Res. Des.* **1999**, *77* (5), 372–384. https://doi.org/10.1205/026387699526359.

(45) Johnson, A. I.; Besik, F.; Hamielec, A. E. Mass Transfer from a Single Rising Bubble. *The Canadian Journal of Chemical Engineering* **1969**, *47* (6), 559–564. https://doi.org/10.1002/cjce.5450470615.

(46) Clift, R.; Grace, J. R.; Weber, M. E. *Bubbles, Drops, and Particles*; Academic Press: New York, 1978.

(47) Robinson, D. B.; Peng, D.-Y. *The Characterization of the Heptanes and Heavier Fractions for the GPA Peng-Robinson Programs*; Research Report 28; Gas Processors Association: Tulsa, 1978.
(48) Peng, D.-Y.; Robinson, D. B. A New Two-Constant Equation of State. *Ind. Eng. Chem. Fund.* **1976**, *15* (1), 59–64. https://doi.org/10.1021/i160057a011.
(49) King, M. B. *Phase Equilibrium in Mixtures*; Danckwerts, P. V., Ed.; International series of monographs in chemical engineering; Pergamon press: Oxford, 1969.
(50) Krichevsky, I. R.; Kasarnovsky, J. S. Thermodynamical Calculations of Solubilities of Nitrogen and Hydrogen in Water at High Pressures. *J. Am. Chem. Soc.* **1935**, *57* (11), 2168–2171. https://doi.org/10.1021/ja01314a036.
(51) Lin, H.; Duan, Y.-Y. Empirical Correction to the Peng–Robinson Equation of State for the Saturated Region. *Fluid Phase Equilibria* **2005**, *233* (2), 194–203. https://doi.org/10.1016/j.fluid.2005.05.008.
(52) Schwarzenbach, R. P.; Gschwend, P. M.; Imboden, D. M. *Environmental Organic Chemistry*, 2nd ed.; John Wiley & Sons, Inc.: Hoboken, 2003.
(53) Pedersen, K.S.; Christensen, P. L.; Shaikh, J.A. *Phase Behavior of Petroleum Reservoir Fluids*, 2nd ed.; CRC Press: Boca Raton, 2014.
(54) Danesh, A. *PVT and Phase Behaviour of Petroleum Reservoir Fluids*, Elsevier.; Developments in Petroleum Science; Amsterdam, 1998.
(55) Firoozabadi, A.; Ramey, H. J. Surface Tension of Water-Hydrocarbon Systems at Reservoir Conditions. *J. Can. Petrol. Technol.* **1988**, *27* (03), 41–48. https://doi.org/10.2118/88-03-03.
(56) Hayduk, W.; Laudie, H. Prediction of Diffusion Coefficients for Nonelectrolytes in Dilute Aqueous Solutions. *AIChE J.* **1974**, *20* (3), 611–615. https://doi.org/10.1002/aic.690200329.
(57) Michelsen, M. L.; Mollerup, J. M. *Thermodynamic Models: Fundamentals & Computational Aspects*, 2nd ed.; Tie-Line Publications: Holte, 2007.
(58) Gill, A. E. *Atmosphere-Ocean Dynamics*; International Geophysics Series; Academic Press: New York, 1982.
(59) Sharqawy, M. H.; Lienhard, J. H.; Zubair, S. M. Thermophysical Properties of Seawater: A Review of Existing Correlations and Data. *Desalin. Water Treat.* **2010**, *16* (1–3), 354–380. https://doi.org/10.5004/dwt.2010.1079.
(60) McCain, W. D. *The Properties of Petroleum Fluids*; PennWell Books, 1990.
(61) Poling, B. E.; Prausnitz, J. M.; O'Connell, J. P. *The Properties of Gases and Liquids*, 5th ed.; McGraw-Hill, 2001.
(62) Gros, J.; Dissanayake, A. L.; Daniels, M. M.; Barker, C. H.; Lehr, W.; Socolofsky, S. A. Oil Spill Modeling in Deep Waters: Estimation of Pseudo-Component Properties for Cubic Equations of State from Distillation Data. *Mar. Pollut. Bull.* **2018**, *137*, 627–637. https://doi.org/10.1016/j.marpolbul.2018.10.047.
(63) Young, A. F.; Pessoa, F. L. P.; Ahón, V. R. R. Comparison of Volume Translation and Co-Volume Functions Applied in the Peng-Robinson EoS for Volumetric Corrections. *Fluid Phase Equilibria* **2017**, *435*, 73–87. https://doi.org/10.1016/j.fluid.2016.12.016.
(64) National Oceanographic and Atmospheric Administration OilLibrary github repository https://github.com/NOAA-ORR-ERD/OilLibrary (accessed Apr 17, 2020).
(65) Brewer, P. G.; Peltzer, E. T.; Friederich, G.; Rehder, G. Experimental Determination of the Fate of Rising CO_2 Droplets in Seawater. *Environ. Sci. Technol.* **2002**, *36* (24), 5441–5446. https://doi.org/10.1021/es025909r.
(66) Walz, P.; Brewer, P.; Pelzer, E. Monterey Bay Aquarium Research Institute, Moss Landing, CA, United States. Personal Communication, 2014 and 2020.
(67) Socolofsky, S. A.; Adams, E. E.; Sherwood, C. R. Formation Dynamics of Subsurface Hydrocarbon Intrusions Following the *Deepwater Horizon* Blowout. *Geophys. Res. Lett.* **2011**, *38* (9), L09602. https://doi.org/10.1029/2011GL047174.

(68) Aliseda, A.; Bommer, P.; Espina, P.; Flores, O.; Lasheras, J. C.; Lehr, B.; Leifer, I.; Possolo, A.; Riley, J.; Savas, O.; Shaffer, F.; Wereley, S.; Yapa, P. *Deepwater Horizon Release Estimate by PIV*; National Incident Command Flow Rate Technical Group, 2010; p 215.

(69) Reddy, C. M.; Arey, J. S.; Seewald, J. S.; Sylva, S. P.; Lemkau, K. L.; Nelson, R. K.; Carmichael, C. A.; McIntyre, C. P.; Fenwick, J.; Ventura, G. T.; Mooy, B. A. S. V.; Camilli, R. Composition and Fate of Gas and Oil Released to the Water Column during the *Deepwater Horizon* Oil Spill. *PNAS* **2012**, *109* (50), 20229–20234. https://doi.org/10.1073/pnas.1101242108.

(70) Ryerson, T. B.; Camilli, R.; Kessler, J. D.; Kujawinski, E. B.; Reddy, C. M.; Valentine, D. L.; Atlas, E.; Blake, D. R.; de Gouw, J.; Meinardi, S.; Parrish, D. D.; Peischl, J.; Seewald, J. S.; Warneke, C. Chemical Data Quantify *Deepwater Horizon* Hydrocarbon Flow Rate and Environmental Distribution. *PNAS* **2012**, *109* (50), 20246–20253. https://doi.org/10.1073/pnas.1110564109.

(71) BP Gulf Science Data. Chemistry data associated with water column samples collected in the Gulf of Mexico from May 2010 through July 2012. Available at: https://data.gulfresearchinitiative.org/data/BP.x750.000:0016#distributionInfo (accessed Aug 3, 2017).

(72) French McCay, D. *Data Source for Blowout Modeling Analysis – Daily Dispersant Application Volumes. DWH NRDA Water Column Technical Working Group; Memo to Deepwater Horizon NRDA File. Prepared for National Oceanic and Atmospheric Administration by RPS ASA, South Kingstown, RI, USA. August 26, 2015. Administrative Record No. DWH-AR0103665.Pdf [Https://Www.Fws.Gov/Doiddata/Dwh-Ar-Documents/925/DWH-AR0103665.Pdf; BP Dispersant Volumes Logs: Https://Www.Diver.Orr.Noaa.Gov/Documents/20233/39182/BP+Dispersant+Volumes+Logs.Zip/6c33d118-B946-584b-3ece-D7b2e6b3a467]*; 2015.

(73) Zhao, L.; Boufadel, M. C.; Socolofsky, S. A.; Adams, E.; King, T.; Lee, K. Evolution of Droplets in Subsea Oil and Gas Blowouts: Development and Validation of the Numerical Model VDROP-J. *Mar. Pollut. Bull.* **2014**, *83* (1), 58–69. https://doi.org/10.1016/j.marpolbul.2014.04.020.

(74) Riazi, M. R. *Characterization and Properties of Petroleum Fractions*; ASTM International, 2005.

(75) Wang, B.; Lai, C. C. K.; Socolofsky, S. A. Mean Velocity, Spreading and Entrainment Characteristics of Weak Bubble Plumes in Unstratified and Stationary Water. *J. Fluid Mech.* **2019**, *874*, 102–130. https://doi.org/10.1017/jfm.2019.461.

(76) Jaggi, A.; Snowdon, R. W.; Stopford, A.; Radović, J. R.; Oldenburg, T. B. P.; Larter, S. R. Experimental Simulation of Crude Oil-Water Partitioning Behavior of BTEX Compounds during a Deep Submarine Oil Spill. *Organic Geochemistry* **2017**, *108*, 1–8. https://doi.org/10.1016/j.orggeochem.2017.03.006.